Nano Energy 144 (2025) 111404

Contents lists available at ScienceDirect

Nano Energy

journal homepage: www.elsevier.com/locate/nanoen

Full paper

# π-Conjugation extended phenazinization of natural prosthetic group pyrroloquinoline quinone disodium salt for long-lifespan biomimetic aqueous redox flow batteries

Guochun Ding, Qianchuan Yu, Pengbo Zhang, Yuzhu Liu, Zuoao Wu, Sheng Wen, Tianyu Shen, Zuoxiu Tie, Zhong Jin *

*State Key Laboratory of Coordination Chemistry, MOE Key Laboratory of Mesoscopic Chemistry, MOE Key Laboratory of High Performance Polymer Materials and Technology, Jiangsu Key Laboratory of Advanced Organic Materials, Suzhou Key Laboratory of Green Intelligent Manufacturing of New Energy Materials and Devices, Tianchang New Materials and Energy Technology Research Center, Institute of Green Chemistry and Engineering, School of Chemistry and Chemical Engineering, Nanjing University, Nanjing, Jiangsu 210023, PR China*

ARTICLE INFO

*Keywords:*
Nature produced prosthetic groups
Diamine-dicarbonyl condensation cyclization
Aromatic fused-ring extension
Water-soluble redox-active phenazine-based structure compounds
Aqueous organic redox flow batteries

ABSTRACT

Aqueous organic redox flow batteries (AORFBs) have emerged as a promising candidate for high-safety, cost-efficient, and environment-friendly energy storage. However, the employment of natural organic electroactive molecules in AORFBs remains significantly constrained. Pyrroloquinoline quinone disodium salt (PQQ), as a prototypical oxidoreductase auxiliary group, exhibits superior aqueous solubility and biocompatibility, but the instability of its two ortho-carbonyl groups restricts its application in AORFBs. Herein, we report an efficient π-conjugation extended phenazinization strategy based on diamine-dicarbonyl condensation cyclization reaction to extend the aromatic fused-ring system of PQQ, yielding two water-soluble and redox-active N-heterocyclic compounds, namely PQQPS and PQQPC. After extending the π-conjugation structure, the redox potentials of them demonstrate favorable negative shifts exceeding 330 mV. Moreover, the asymmetrical molecular configurations and highly polar sulfonic/carboxylic groups significantly enhance the aqueous solubility of PQQPS and PQQPC to 1.28 and 1.42 M, respectively. Theoretical simulations and spectroscopic analyses unequivocally demonstrate that PQQPS and PQQPC exhibited excellent stability during cycling. Consequently, the as-fabricated AORFBs with a high concentration of 0.5 M exhibit a specific capacity of 22.63 Ah $L^{-1}$, an output power density of 0.205 W $cm^{-2}$, and a capacity retention of 97.5 % over 800 cycles (i.e. 99.996 % $cycle^{-1}$ or 99.85 % $day^{-1}$). This work highlights the great potential of π-conjugation extension strategy based on amine-carbonyl condensation reactions to boost the overall performances of bio-derived or nature-inspired molecules towards sustainable and long-cycling AORFBs.

## 1. Introduction

Electrochemical energy storage systems have emerged as a strategic imperative in responding to the energy transition and sustainable development [1–10]. Aqueous organic redox flow batteries (AORFBs) is a promising contender for grid-scale energy storage, offering high safety and superior sustainability characteristics [11–14]. It is meaningful to develop redox-active organic molecules endowed with widespread sources and cost-effectiveness for AORFBs [15–23]. However, there are still very limited reports about naturally derived organic molecules, apart from those utilizing flavin mononucleotide (FMN) and several natural dyes [24–27]. Pyrroloquinoline quinone disodium salt (PQQ), being a typical prosthetic group with physiological functions akin to vitamins, is mainly obtained from biological fermentation and chemical synthesis method. Although PQQ exhibits ideal aqueous solubility in neutral and alkaline solutions, its stability in electrochemical processes is compromised by the tautomerization reactions of its two adjacent carbonyl groups.

Herein, we report an effective π-conjugation extended phenazinization modification via single-step coupling reactions, and synthesized two heteroaromatic fused-ring derivatives of PQQ, namely, 6-carboxy-10-sulfo-5H-pyrido[2,3-*a*]pyrrolo[2,3-*c*]phenazine-2,4-dicarboxylate

* Corresponding author.
*E-mail address:* zhongjin@nju.edu.cn (Z. Jin).

https://doi.org/10.1016/j.nanoen.2025.111404
Received 18 May 2025; Received in revised form 18 July 2025; Accepted 19 August 2025
Available online 20 August 2025

sodium (PQQPS) and 6,10-dicarboxy-5H-pyrido[2,3-*a*]pyrrolo[2,3-*c*] phenazine-2,4-dicarboxylate sodium (PQQPC). The as-obtained PQQPS and PQQPC molecules exhibit more negative redox potentials which were shifted by over 330 mV. Through introducing the carboxylic or sulfonic groups as highly polar moieties, PQQPS or PQQPC with the asymmetrical configuration and multiple hydrophilicity groups is able to achieve a high solubility (1.28 and 1.42 M, respectively) in the alkaline environment with an ionic dissociation behavior. Compared with the original PQQ molecule, PQQPS and PQQPC with modified N-heterocyclic fused-ring system greatly expand the molecule dimension and π conjugation, resulting them more stable cycling performance. Coupled with the ferro/ferrocyanide catholyte, the as-assembled AORFBs with a high concentration of 0.5 M (i.e., 1.0 M electron concentration) exhibit an extremely low capacity fade rate of 0.004 % cycle$^{-1}$ (equivalent to 0.15 % day$^{-1}$) over 800 cycles and outstanding output power density of 0.205 W cm$^{-2}$. Furthermore, a comprehensive set of spectroscopic tests unequivocally corroborate the stability of PQQPS and PQQPC under high temperature conditions and during long-term cycling processes. The proposed π-conjugation extended phenazinization strategy via amine-carbonyl condensation reactions in this work can effectively enhances the water solubility and electrochemical performances of numerous bio-inspired compounds, laying a robust foundation for groundbreaking advancements in AORFBs.

## 2. Result and discussion

Redox-active organic materials with abundant resource and structural tunability, offer great potential in AORFBs. Conventional molecular engineering strategies primarily focus on dual optimization of aqueous solubility enhancement and molecular stabilization to achieve high-energy-density AORFBs. PQQ, as a redox coenzyme, is widely used in biomedicine and food fields. While the ortho-positioned dual carbonyl groups in PQQ confer redox activity, their structural instability during charge-discharge process persists as a critical limitation. To overcome the problem, we employed a π-conjugation extended phenazinization strategy to convert quinone-based structure into phenazine-based structure. The synthetic pathway was illustrated in Fig. 1a. Through a convenient diamine-dicarbonyl condensation synthesis

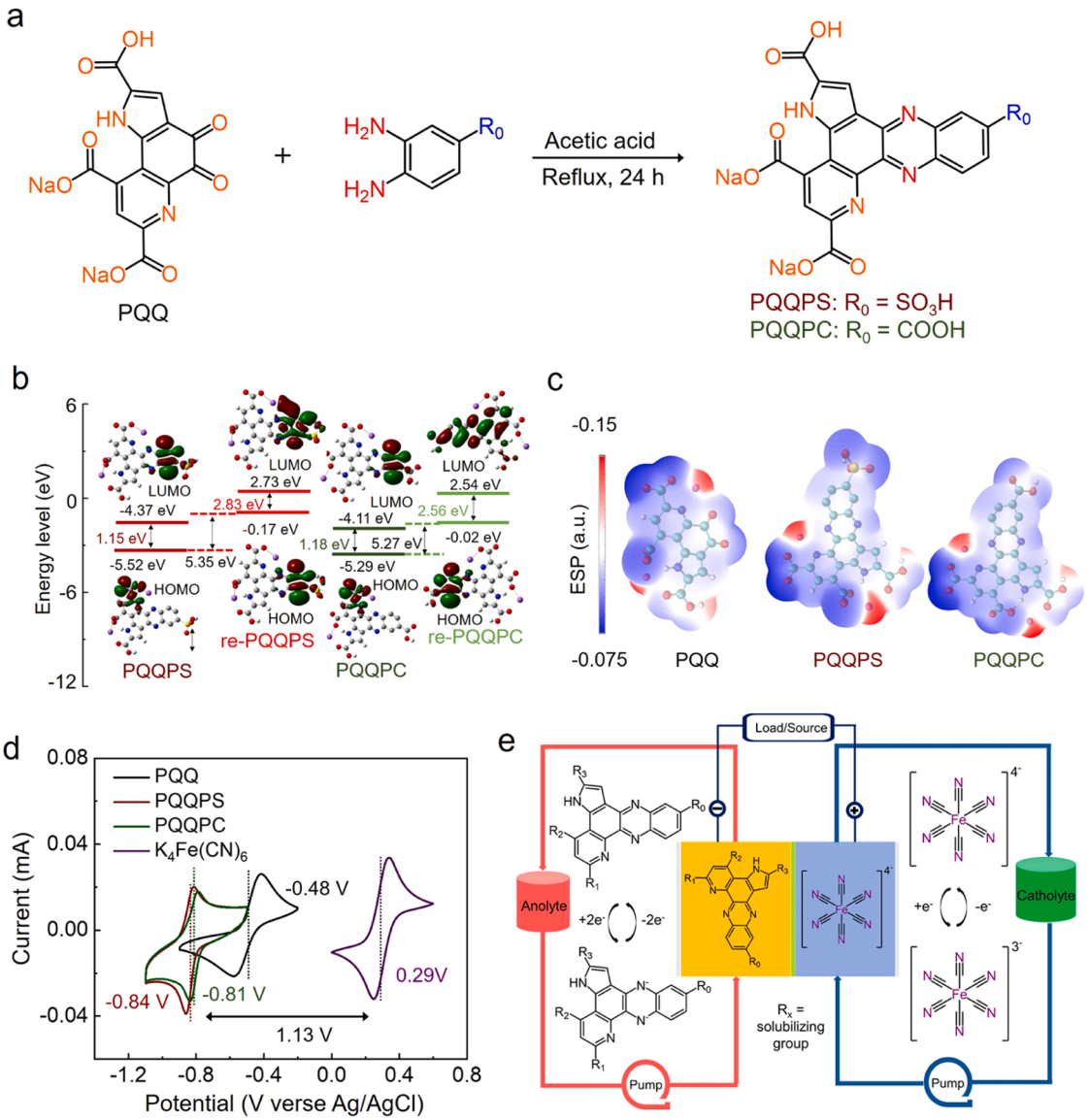


**Fig. 1.** (a) Synthesis route of PQQPS and PQQPC via diamine-dicarbonyl condensation cyclization reactions of PQQ. (b) Molecular orbitals and energy gaps of PQQPS and PQQPC at oxidized and reduced states. (c) Optimized structures and electrostatic potentials of PQQ, PQQPS and PQQPC. (d) CV curves of PQQPS, PQQPC, PQQ, and $K_4Fe(CN)_6$ in 1.0 M KOH solution at a scanning rate of 100 mV s$^{-1}$. (e) Schematic diagram of the AORFBs based on PQQPS or PQQPC anolyte and $K_4Fe(CN)_6$ catholyte.

routes, two benzosulfated and benzocarboxylated PQQ derivatives, namely PQQPS and PQQPC, were massively synthesized by refluxing in acetic acid for 24 h, with an ultrahigh yield of almost 100 %. In contrast to conventional synthesis routes, the synthesis approach proposed in this study stands out for its utilization of nature-inspired precursors, convenient streamlined one-step processes, and high yields. Detailed synthesis procedures are available in the Supporting Information section. The production of PQQPS and PQQPC was proved by $^{1}H$ and $^{13}C$ nuclear magnetic resonance (NMR) characterizations, as shown in Figure S1–S4.

The highest occupied molecular orbital (HOMO) and lowest unoccupied molecular orbital (LUMO) of PQQPS and PQQPC in their oxidized and reduced states were meticulously analyzed (Fig. 1b). The LUMO energy levels of PQQPS and PQQPC reveal a similarity, as do the HOMO energy levels of their reduced counterparts (re-PQQPS and re-PQQPC), suggesting the analogous redox potentials displayed by PQQPS and PQQPC. Further analysis manifests that the energy gap between the HOMO levels of PQQPS and re-PQQPS stands at 5.35 eV, which is approximately equal to that between PQQPC and re-PQQPC (5.27 eV). This indicates a similar energy barrier for the reduction step of them. Additionally, the HOMO-LUMO energy gap widens for re-PQQPS and re-PQQPC relative to their oxidized forms, PQQPS and PQQPC. This broadened energy gap implies a reduction in electron conductivity in their reduced states, aligning with the decrease in aromaticity[28,29]. Furthermore, we utilized DFT simulations to obtain optimized structures and electrostatic potentials (ESP) for PQQ, PQQPS and PQQPC. As shown in Fig. 1c, the ESPs of PQQPS and PQQPC were more negative than that of PQQ. The deprotonation of carboxylate and sulfonate groups could induce an asymmetric charge distribution and higher polarizability, thereby enhancing intermolecular interactions and improving solubility.

The electrochemical behavior of PQQPS and PQQPC in 1.0 M KOH solution was investigated by cyclic voltammetry (CV). Both PQQPS and PQQPC exhibited one pair of sharp redox peak, corresponding to the redox potentials of −0.84 V and −0.81 V for them (vs. Ag/AgCl), respectively (Fig. 1d). However, PQQ exhibited a higher redox peak at −0.48 V [30]. The reduced redox potential in PQQPS and PQQPC can be attributed to the size extension of π-conjugated rings, which increased the electron-donating effect of benzene rings, resulting in a negative shift in redox potential relative to the phenazine core. Moreover, the redox peak separation of both PQQPS and PQQPC is ~84 mV, indicating their lower polarization than that of PQQ (140 mV). The structural configuration and stack design of AORFBs based on PQQPS or PQQPC anolyte and $K_4Fe(CN)_6$ catholyte were shown in Figure 1e and S5. By pairing with $K_4Fe(CN)_6$ catholyte, the full AORFBs presented an open-circuit voltage (OCV) exceeding 1.1 V. The Pourbaix diagrams derived from the CV curves measured at various pH levels demonstrated that the relevant slopes for PQQPS and PQQPC (−59.3 and

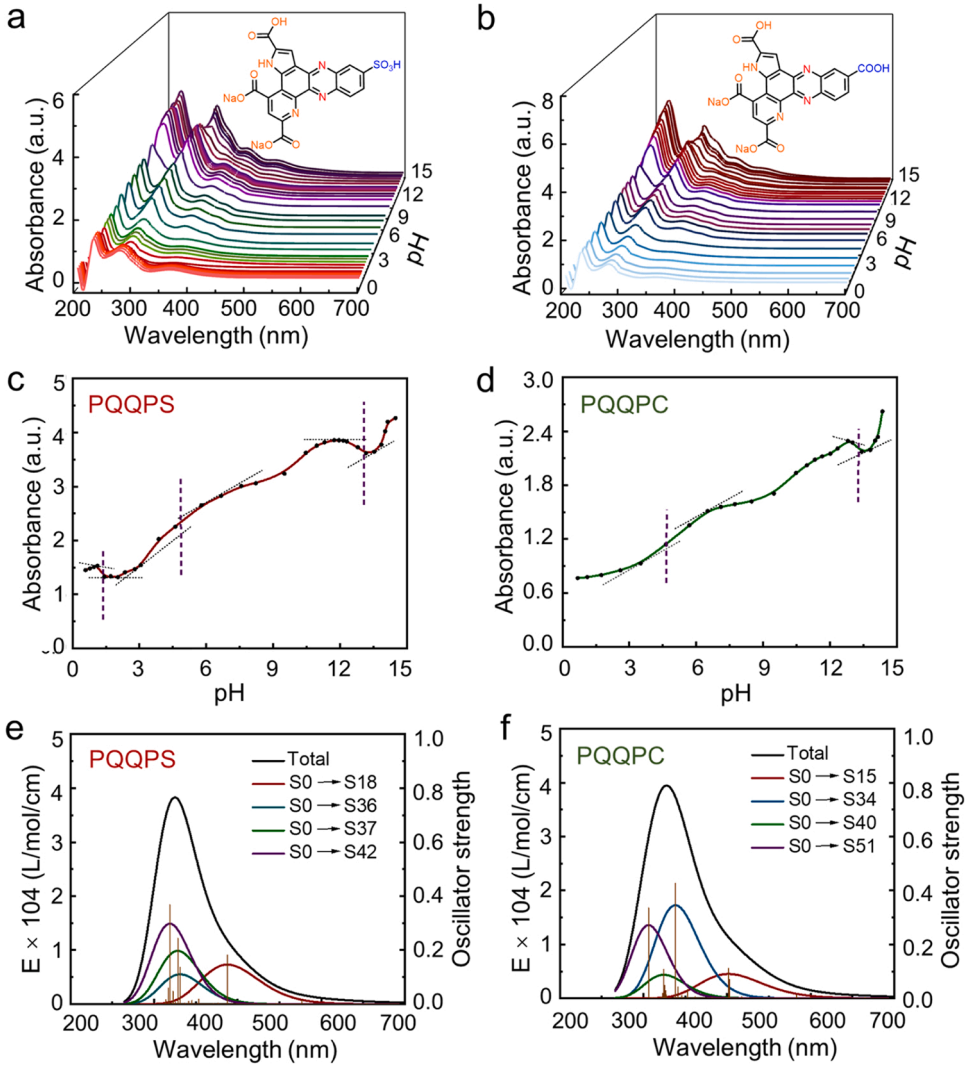


**Fig. 2.** (a, b) UV-Vis absorption spectra of (a) PQQPS and (b) PQQPC at different pH values. (c, d) Absorption wavelength versus pH value plots of (c) PQQPS and (d) PQQPC at $\lambda_{306nm}$. (e, f) Simulated UV-Vis absorption spectra of (e) PQQPS and (f) PQQPC calculated by TDDFT method at the B3LYP/6–31 G(d,p) level.

−59.8 mV $pH^{-1}$) exhibited a close approximation to the theoretical value (−59.2 mV $pH^{-1}$) [31], corresponding to a two-electron/two-proton process (Figure S6). These findings suggest that the fused-ring extended phenazinization of PQQ molecule leads to a reduced redox potential and enhanced reversibility, both of which are advantageous in attaining superior electrochemical performance in alkaline AORFBs.

The pH-dependent physiochemical properties of PQQPS and PQQPC were investigated by UV-Vis absorption spectra at different pH values. For both PQQPS and PQQPC, the absorbance peak exhibited a red shift from $\lambda_{285nm}$ under pH 7 to $\lambda_{306nm}$ under pH 14 (Fig. 2a-b and Figure S7). It is worth noting that the peak around 250 nm belong to KOH. According to the absorbance wavelength versus pH value plots (Figs. 2c-2d), PQQPS exhibited three $pK_a$ values approximately 1.49, 4.62 and 13.38. Conversely, PQQPC exhibited two $pK_a$ values approximately 4.58 and 13.38. These values correspond to the dissociation process involving sulfonic acid, carboxylic acid groups, as well as the protonation of hydrogen within the pyrrole ring. Based on UV-Vis absorbance measurements, the maximum solubilities of PQQPS, PQQPC and PQQ in 1.0 M KOH solutions were determined to be 1.28, 1.42 and 0.75 M, respectively (Figure S8). In addition, time-dependent density functional theory (TDDFT) calculations were performed to calculate the energy levels of HOMO and LUMO for simulating the UV-Vis absorption properties of PQQPS and PQQPC (Fig. 2e-f). Notably, when the wavelength exceeds 330 nm, both PQQPS and PQQPC exhibit weak absorption intensities. Consequently, the simulated UV-Vis absorbance spectra featured one single prominent and sharp peak. The absorption peaks at 387.9 nm and 402.6 nm arose from the electron transition from HOMO to LUMO. In the spectrum of PQQPS, the S0→S18 excitation contributes marginally to the peak at 387.9 nm, while in the spectrum of PQQPC, the S0→S15 excitation makes a similar minor contribution to the peak at 402.6 nm. It is noting that the excited states causing the absorption peak below 350 nm differ between PQQPS and PQQPC. Specifically, the peaks below 350 nm in the UV-Vis absorption spectra of PQQPS and PQQPC were influenced by the S0→S36, S37, S42 and S0→S34, S40, S42 excitations, respectively.

The redox kinetics of PQQPS and PQQPC were determined through linear sweep voltammetry (LSV), as shown in Figure S9−S10. All experiments were conducted in a 1.0 M KOH solution, with a 1.0 mM concentration of the active species. The diffusion coefficient ($D$) could be obtained from the Levich plot of the limiting diffusion currents and the square root of the rotation rates[32–34]. As the rotation rate increased from 300 to 1750 rpm at a scan rate of 25 mV $s^{-1}$ (Figure S9a and S10a), the $D$ values of PQQPS and PQQPC were determined to be $3.12 \times 10^{-6}$ and $2.58 \times 10^{-6}$ $cm^2$ $s^{-1}$, respectively (Figure S9b and S10b). By fitting the Butler-Volmer equation to Levich plots (Figure S9c and S10c), the electron-transfer rate constants ($k_0$) of PQQPS and PQQPC were calculated to be $1.97 \times 10^{-3}$ and $1.82 \times 10^{-3}$ cm $s^{-1}$, respectively (Figure S9d and S10d). As the scan rate increased from 25 to 100 mV $s^{-1}$, both the oxidation and reduction peak currents had a linear relationship with the square root of the scan rate ($\upsilon^{1/2}$), indicating a reversible and diffusion-controlled redox process (Figure S11a and S12a). The slopes of the cathodic and anodic scans were calculated to be virtually identical, suggesting that the oxidized and reduced molecules exhibit comparable diffusion coefficients (Figure S11b and S12b) [35, 36]. Furthermore, the CV curves of PQQPS and PQQPC displayed excellent overlap and were devoid of additional peaks throughout 50 cycles, thereby indicating the absence of side reactions and remarkable electrochemical reversibility (Figure S11c and S12c).

The working performances of as-prepared AORFBs coupled by two derivative anolytes and excess $K_4Fe(CN)_6$ catholyte were firstly measured at low concentrations (Fig. 3). The electrolytes consist of 15 mL of 0.2 M catholyte and 5 mL of 0.05 M anolyte, respectively. A polybenzimidazole (PBI) membrane was employed as the separator between catholyte and anolyte. Electrochemical impedance spectroscopy revealed that the impedance of PBI separator in 1.0 M KOH solution was 0.42 Ω $cm^2$ (Figure S13a). Furthermore, the permeability values of PQQPS and PQQPC solutions through this separator were remarkably low, registering as $8.17 \times 10^{-11}$ and $7.31 \times 10^{-11}$ $cm^2$ $s^{-1}$, respectively (Figure S13b). Both PQQPS and PQQPC based AORFBs delivered an open-circuit voltage exceeding 1.1 V, which was in agreement with CV results. As shown in Fig. 3a–b, the $K_4Fe(CN)_6$||PQQPS AORFB exhibited a discharge capacity of 2.46 and 2.22 Ah $L^{-1}$ at 50 and 100 mA $cm^{-2}$, and the $K_4Fe(CN)_6$||PQQPC AORFB exhibited a discharge capacity of 2.38 and 2.11 Ah $L^{-1}$ at 50 and 100 mA $cm^{-2}$, respectively. The polarization curves of $K_4Fe(CN)_6$||PQQPS and $K_4Fe(CN)_6$||PQQPC AORFBs were measured by LSV at different SOCs of 20 %, 50 % and 100 % (Fig. 3c–d). The power density reached around 100 mW $cm^{-2}$ at 100 % SOC both for them. Upon a galvanostatic cycling process at 80 mA $cm^{-2}$ between 0.6–1.6 V, the $K_4Fe(CN)_6$||PQQPS AORFB exhibited a discharge capacity of 2.44 Ah $L^{-1}$ without capacity decay for 1600 cycles (equivalent to 4.5 days), which is 91.04 % of its theoretical capacity (2.68 Ah $L^{-1}$) (Fig. 3e). Similarly, the $K_4Fe(CN)_6$||PQQPC AORFB exhibited no capacity fade after 1600 cycles (equivalent to 3 days) with a discharge capacity of 2.34 Ah $L^{-1}$, which is 87.31 % of its theoretical capacity. The Coulombic efficiencies remained consistently close to 100 %, while the energy efficiencies reached to > 75 % during the cycling processes. In comparison, the discharge capacity of PQQ dramatically decreased from 2.45 to 1.21 Ah $L^{-1}$ just after 300 cycles. For the galvanostatic-potentiostatic cycle tests, the AORFBs were first charged with the potential held at 1.4 V (for PQQPS and PQQPC) or 1.0 V (for PQQ) at 80 mA $cm^{-2}$ until the current density decreased to 5 mA $cm^{-2}$ and then were discharged with the potential held at 0.6 V at 80 mA $cm^{-2}$ until the current density decreased to 5 mA $cm^{-2}$ (Fig. 3f). For PQQPS and PQQPC, the discharge capacities maintained unaltered after 800 cycles (equivalent to 8.5 and 7 days). However, obvious capacity loss was observed for PQQ after 500 cycles. Such substantial capacity decline is attributed to the instability of ortho-carbonyl groups that are prone to tautomerization during the redox processes (Figure S14) [37]. The galvanostatic charge-discharge plateaus of PQQPS and PQQPC at the 1600th cycle was almost overlapped with those at the 1st cycle (Figure S15), indicating their favorable long-term stability. At elevated concentrations of 0.1 M and 0.25 M anolytes, no capacity decline was observed for PQQPS and PQQPC after 600 and 500 cycles at 80 mA $cm^{-2}$ (Figure S16–S18).

The long-cycling performances of PQQPS based AORFBs at a higher concentration of 0.5 M were supplemented in Fig. 4. The anolyte is 4 mL of 0.5 M PQQPS in 1.0 M KOH solution, and the catholyte is 50 mL of 0.4 M $K_4Fe(CN)_6$ in 1.0 M KOH solution. At different current densities of 20, 40, 80, 100 and 120 mA $cm^{-2}$ (Fig. 4a–b), the discharge capacities of $K_4Fe(CN)_6$||PQQPS AORFB were 24.54, 23.23, 22.22, 21.92, and 21.12 Ah $L^{-1}$, and corresponding energy efficiency values were 88.8 %, 83.6 %, 75.5 %, 71.3 %, and 66.9 %, respectively. When the current density returned to 20 mA $cm^{-2}$, the discharge capacity restored to its initial value. Fig. 4c showed the OCVs of PQQPS at different state of charges (SOCs). The OCVs at 50 % SOC were measured to be 1.13 V for PQQPS, and reached 1.29 V at 100 % SOC, which is competitive among the existing AORFBs based on phenazine derivatives. The polarization curves were recorded by LSV at different SOCs of 20 %, 50 % and 100 % (Fig. 4d). At 100 % SOC, the peak power density was 0.175 W $cm^{-2}$. The $K_4Fe(CN)_6$||PQQPS AORFB worked at 80 mA $cm^{-2}$ between 0.4–1.6 V delivered a specific capacity of 22.63 Ah $L^{-1}$ after circulating for 800 cycles (equivalent to 18 days), which is 84.4 % of its theoretical capacity (26.8 Ah $L^{-1}$). The capacity retention was 97.5 %, corresponding to a capacity fade rate of 0.003 $cycle^{-1}$ or 0.13 % $day^{-1}$ (Fig. 4e). During the entire cycling process, the Coulombic efficiency maintained a near-perfect 100 %, while the energy efficiency surpassed 70 %. The high capacity retentions at both low and high concentrations suggest that the stability of PQQPS is not significantly influenced by varying concentrations. The corresponding energy density of $K_4Fe(CN)_6$||PQQPS AORFB was calculated to be 25.57 Wh $L^{-1}$, and its theoretical and practical energy density was calculated to be 19.09 and 14.61 Wh $L^{-1}$

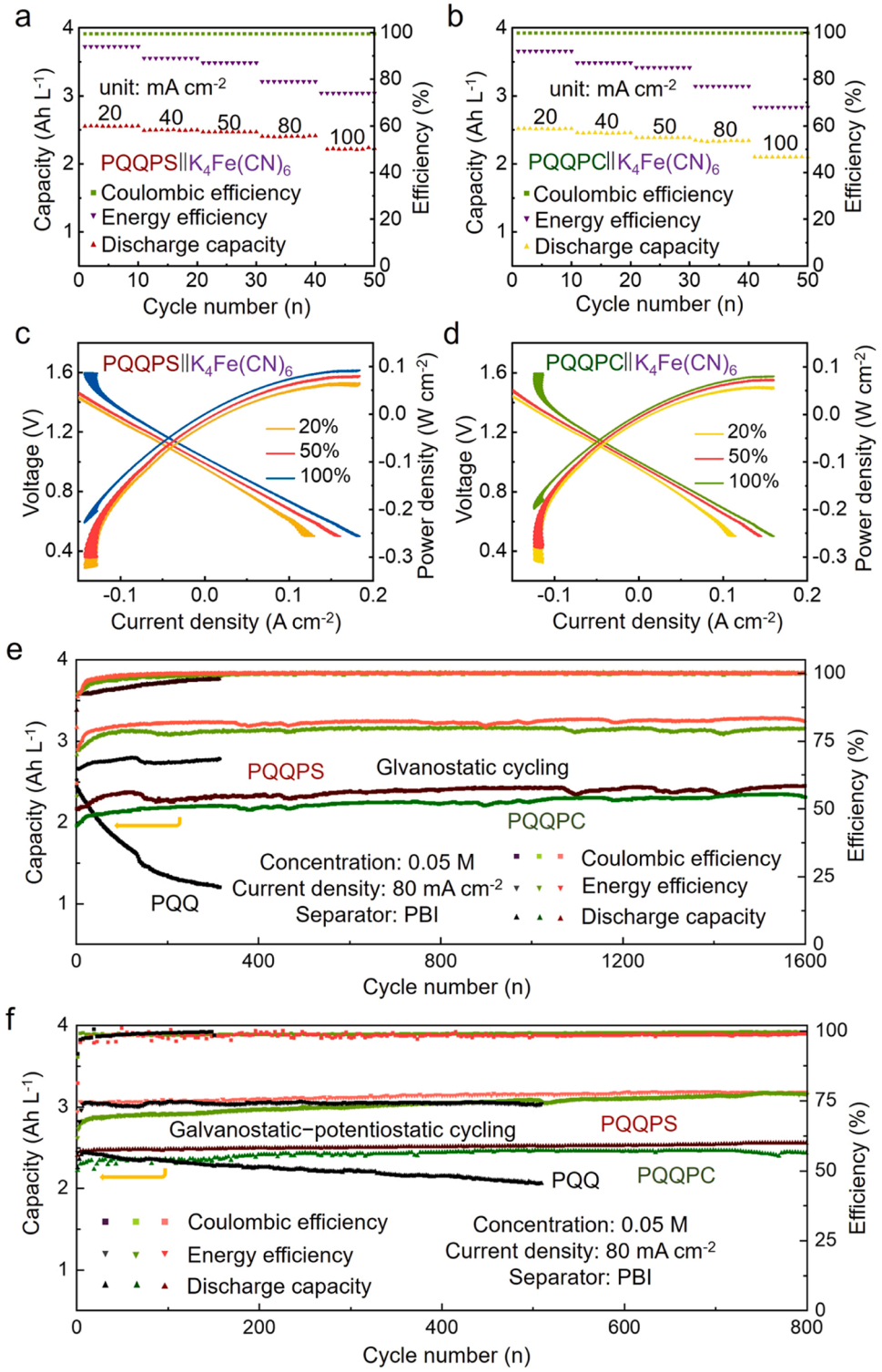


**Fig. 3.** Electrochemical performances of as-fabricated AORFBs at low concentrations. (a, b) Discharge capacity, Coulombic efficiency and energy efficiency of (a) $K_4Fe(CN)_6$||PQQPS and (b) $K_4Fe(CN)_6$||PQQPC AORFBs at different current densities of 20, 40, 50, 80 and 100 mA $cm^{-2}$, respectively. (c, d) Polarization and power density curves of (c) $K_4Fe(CN)_6$||PQQPS and (d) $K_4Fe(CN)_6$||PQQPC AORFBs at 20 %, 50 % and 100 % SOCs, respectively. (e) Galvanostatic cycling performance of $K_4Fe(CN)_6$||PQQPS, $K_4Fe(CN)_6$||PQQPC and $K_4Fe(CN)_6$||PQQ AORFBs at 80 mA $cm^{-2}$ between 0.6 and 1.6 V. (f) Galvanostatic-potentiostatic cycling performance of $K_4Fe(CN)_6$||PQQPS, $K_4Fe(CN)_6$||PQQPC and $K_4Fe(CN)_6$||PQQ AORFBs at 80 mA $cm^{-2}$. The AORFBs were charged with the potential held at 1.4 V (for PQQPS and PQQPC) or 1.0 V (for PQQ) at 80 mA $cm^{-2}$ until the current density decreased to 5 mA $cm^{-2}$, and then were discharged with the potential held at 0.6 V until the current density decreased to 5 mA $cm^{-2}$.

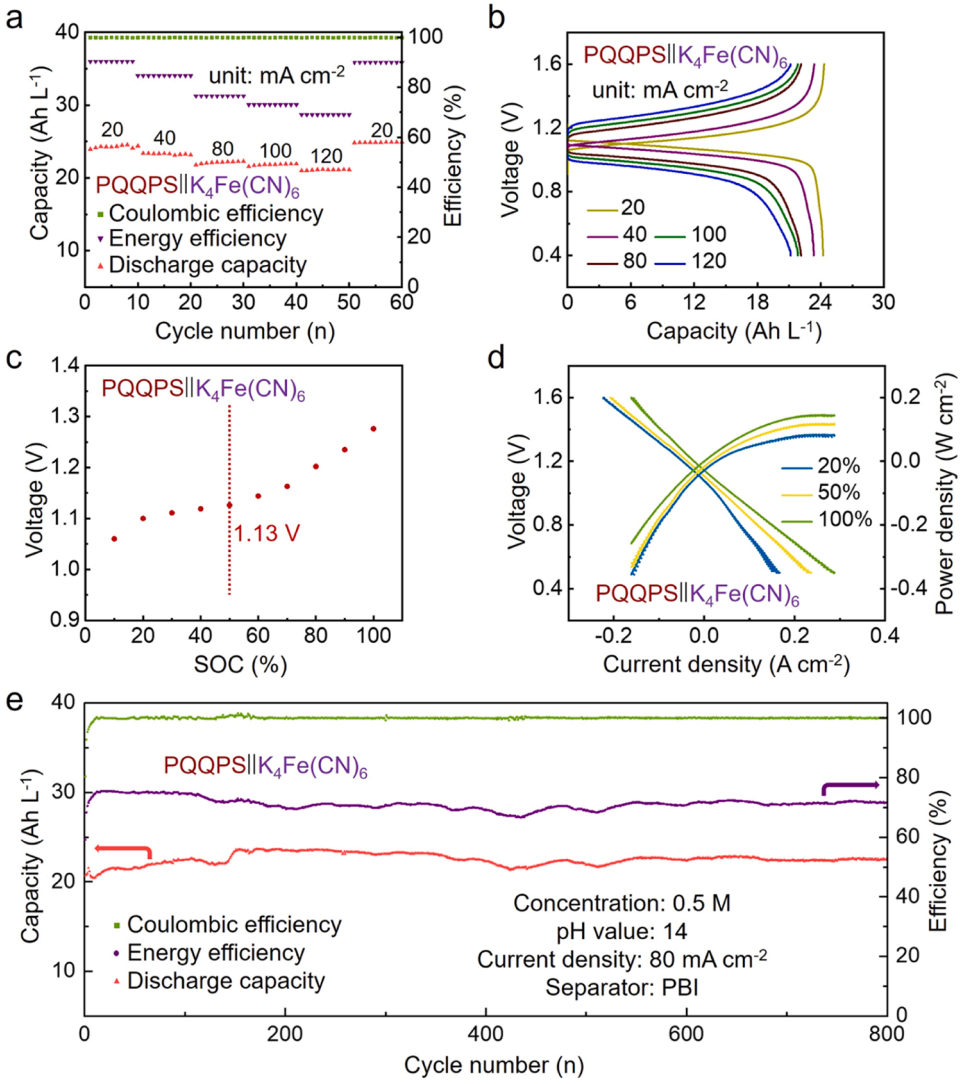


**Fig. 4.** Electrochemical performances of PQQPS-based AORFBs at high concentrations. (a) Discharge capacity, Coulombic efficiency and energy efficiency of $K_4Fe(CN)_6$||PQQPS AORFB at different current densities. (b) Galvanostatic charge-discharge curves of $K_4Fe(CN)_6$||PQQPS AORFB at different current densities of 20, 40, 50, 80, and 100 mA $cm^{-2}$, respectively. (c) Open-circuit voltages at different SOCs for PQQPS. (d) Polarization and power density curves of $K_4Fe(CN)_6$||PQQPS AORFB at 20 %, 50 % and 100 % SOC, respectively. (e) Long-term cycling performance of $K_4Fe(CN)_6$||PQQPS AORFB at a current density of 80 mA $cm^{-2}$ between 0.4 and 1.6 V.

based on the limiting electrode. Figure S19 exhibited the voltage plateaus during long-term cycling process. The discharge voltage plateaus gradually increased and moved closer to the cutoff voltages with increasing cycle count. The continuously increased polarization resulted in less complete discharging and capacity fading[38]. Additionally, the cost of PQQPS and detailed performances of $K_4Fe(CN)_6$||PQQPS AORFB in this study were also compared with other existing phenazine derivative based AORFBs (Table S1 and S2). In view of the efficient synthesis, moderate material cost, and good structural stability, along with the characteristics of nature-inspired PQQ, PQQPS could be considered as a promising candidate for AORFBs [19,24,29,30,38–40].

Through the implementation of a π-conjugation extended phenazinization strategy, we achieved a substantial improvement in the cycling stability for PQQPS and PQQPC. The redox mechanism of them during cycling was studied by in situ UV-Vis absorption analyses (Fig. 5a–c and Figure S20). Upon charging, the color of PQQPS anolyte in 1.0 M KOH solution changed from dark red to black. As the charging process continued, the absorption peak at $\lambda_{360nm}$ and $\lambda_{420nm}$ gradually broadened and disappeared (Fig. 5a). This phenomenon is attributed to the electron acquisition by the N atoms in the pyrazine ring. During the discharging process, the absorption peak at $\lambda_{360nm}$ and $\lambda_{420nm}$ gradually increased (Fig. 5b), corresponding to the electron loss from the N atoms in the pyrazine ring. These reversible changes in peak intensity were shown in Fig. 5c, demonstrating the good redox stability and reversibility of PQQPS. Electron paramagnetic resonance (EPR) spectroscopy analysis was conducted to detect $PQQPS^{3-\bullet}$ radical anion derived from the reduction of $PQQPS^{2-}$ (Fig. 5d). An EPR resonance centered at a G-factor of ~3500 was related to the presence of $PQQPS^{3-\bullet}$ radical anion. As the charging process continued, the EPR signal of $PQQPS^{3-\bullet}$ radical anion reached to its maximum level at 50 % SOC. The signal intensity of $PQQPS^{3-\bullet}$ radical anion decreased at 75 % SOC. No EPR signal was detected at 100 % SOC, indicating the full reduction from $PQQPS^{2-}$ to $PQQPS^{4-}$. The EPR signal associated with $PQQPS3^{-\bullet}$ radical anion exhibited no obvious splitting or hyperfine structure, which is attributed to the broadened signal caused by hyperfine coupling of hydrogen atoms in the center of phenazine.

The stability of PQQPS and PQQPC was conducted by the $^1H$ NMR analyses at an elevated temperature (Fig. 5e and Figure S21) [40,41]. After placing their solution at 80 ℃ for more than 10 days, the $^1H$ NMR spectra exhibited no new proton peaks compared to that of its original

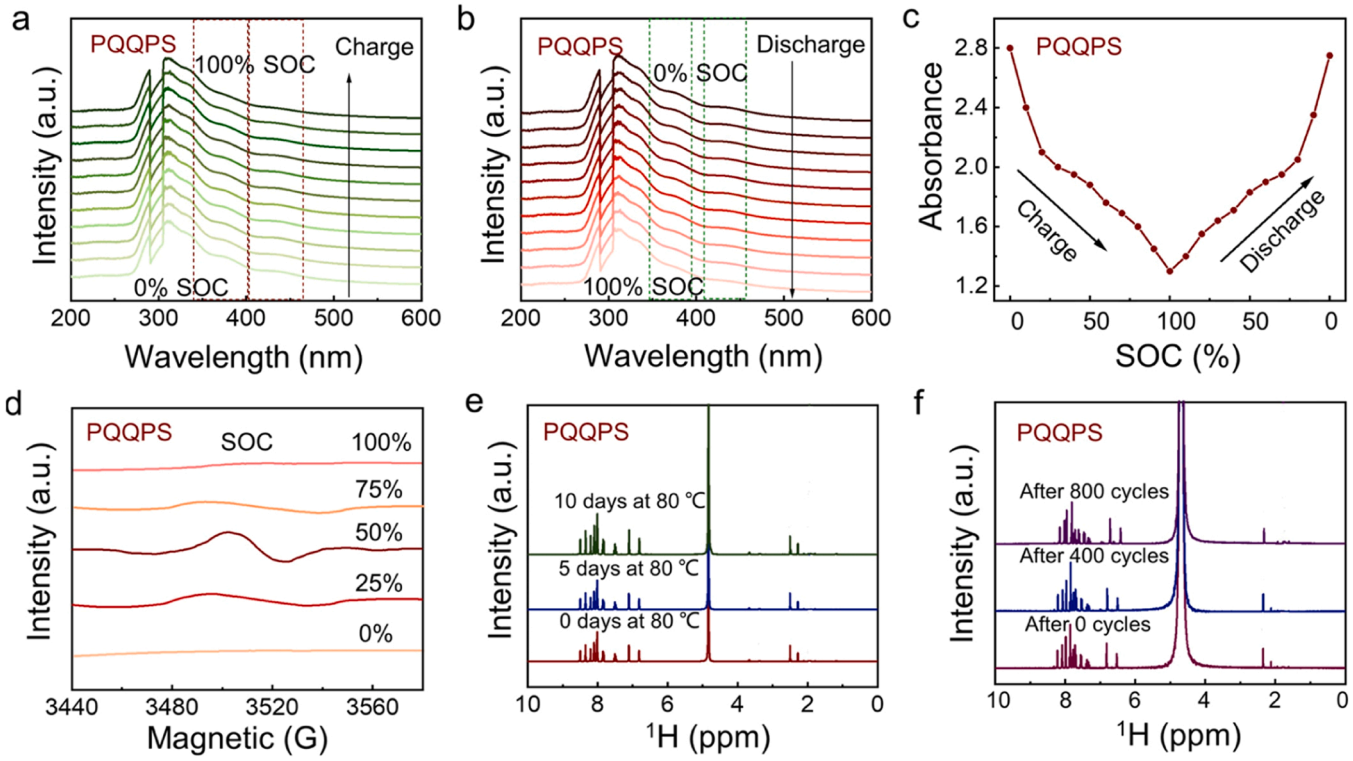


**Fig. 5.** (a, b) In-situ UV-Vis absorption spectra of PQQPS during (a) charging and (b) discharging processes. (c) Light absorbance of PQQPS anolyte at different SOCs. (d) EPR spectra of PQQPS anolyte at different SOCs. (e) $^{1}$H NMR analysis of PQQPS anolyte stored at 80 ℃. (f) $^{1}$H NMR analysis of PQQPS anolyte after different galvanostatic cycles.

state, indicating its excellent thermal and chemical stability. During the long-term cycling at high concentrations, we further analyzed the $^{1}$H NMR spectra of PQQPS anolyte at different galvanostatic cycles. In Fig. 5f and S22a, no obvious change was observed in the $^{1}$H NMR and $^{13}$C NMR spectra. We also analyzed the $^{13}$C NMR spectra of $K_4Fe(CN)_6$ catholyte (Figure S22b). Although the signal became weaker and wider, no impurity signal appeared. It is indicated that $K_4Fe(CN)_6$ exhibited no chemical decomposition during cycling [33]. According to previous literature [40], when carboxylic acid functional groups (-COOH) are linked to aromatic core by chemically inert carbon atom rather than heteroatoms, the possible tautomerization pathway could be excluded. Similarly, PQQPS has considerable conjugation with the solubilizing groups connected to the aromatic core by carbon linkages. What's more, there is no place on the conjugated rings where side reactions such as Michael addition or tautomerization could occur. Therefore, PQQPS molecules can remain highly stable during long-term cycling. In addition, the CV curve of PQQPS anolyte after long cycling still showed its reversible redox properties, and no additional peaks were observed in $K_4Fe(CN)_6$ catholyte (Figure S22c and S22d). These results indicate the absence of decomposition and crossover of PQQPS during cycling. On the other hand, the impedance of PBI separator membrane before and after long-term cycling increased from 0.42 to 0.59 Ω cm$^2$. We believe that the capacity fade could be partially owing to the slight increase of membrane resistance after cycling (Figure S23). The increased membrane resistance enables the charging-discharging plateaus an obvious elevation, resulting in a decreased charging-discharging time and a decreased capacity.

## 3. Conclusion

In summary, we report an effective π-conjugation extended phenazinization strategy to cyclize natural auxiliary group PQQ with o-phenylenediamine derivatives via one-step coupling reactions, yielding two robust and asymmetric compounds, PQQPS and PQQPC. Owing to their large-size N-heterocyclic fused-ring structures, the redox potentials of PQQPS and PQQPC exhibit significant negative shifts. The asymmetric molecular configurations and highly water-solubilizing sulfonic/carboxylic groups significantly enhance their aqueous solubility. Consequently, the AORFBs based on 0.5 M PQQPS anolyte delivered exceptional specific capacity, power density and cycling stability. Comprehensive spectroscopic tests proved their excellent electrochemical and thermal stability, and the capacity fade is primarily attributed to the increase of membrane resistance after cycling. Furthermore, the production cost comparison with other phenazine molecules shows that PQQPS and PQQPC are promising candidates in AOFRBs. The viable π-conjugation extended phenazinization strategy, as a prototypical amine-carbonyl condensation synthesis route, holds significant potential in the synthesis of various organic compounds, enabling the production of multitudinous redox-active derivatives. This work highlights the pivotal potential of nature-inspired molecular design and π-conjugation extension strategy in improving the performance and nurturing the long-cycling capability of AORFBs.

## Supporting information

Supporting Information is available from the author. Experimental section and additional figures and tables, including NMR spectra, UV−vis analyses, CV curves, EIS curves, electrochemical measurements, and battery performance tests; Figures S1−S23 and Table S1−S2.

## Author contributions

The original idea was conceived by Z. J.; the experiments and data analyses were performed by G. C. D., P. B. Z., Y. Z. L., Z. A. W., S. W., and Z. X. T.; the structure characterizations were performed by Q. C. Y., and T. Y. S.; the battery performance measurements were conducted by G. C. D.; the manuscript was drafted by Z. J., and G. C. D. All authors have approved the manuscript.

## CRediT authorship contribution statement

**Guochun Ding:** Writing – review & editing, Writing – original draft, Visualization, Validation, Methodology, Investigation, Formal analysis, Data curation. **Qianchuan Yu:** Visualization, Validation, Software. **Zhong Jin:** Supervision, Resources, Funding acquisition, Conceptualization. **Zuoxiu Tie:** Supervision, Funding acquisition, Conceptualization. **Sheng Wen:** Validation. **Sheng Tianyu:** Validation. **Yuzhu Liu:** Validation, Investigation. **Zuoao Wu:** Validation, Investigation. **Pengbo Zhang:** Validation, Investigation.

## Declaration of Competing Interest

The authors declare that they have no known competing financial interests or personal relationships that could have appeared to influence the work reported in this paper.

## Acknowledgments

The authors are grateful to the National Natural Science Foundation of China (Nos. 22479074, 22475096), The Equipment Pre-Research and Ministry of Education Joint Fund General Project (No. 8091B02052407), the Natural Science Foundation of Jiangsu Province (Nos. BK20240400, BK20241236), The Science and Technology Major Project of Jiangsu Province (No. BG2024013), The Scientific and Technological Achievements Transformation Special Fund of Jiangsu Province (No. BA2023037), The Academic Degree and Postgraduate Education Reforming Project of Jiangsu Province (No. JGKT24_C001), The Key Core Technology Open Competition Project of Suzhou City (No. SYG2024122), The Open Research Fund of Suzhou Laboratory (No. SZLAB-1308-2024-TS005), The Gusu Leading Talent Program of Scientific and Technological Innovation and Entrepreneurship in Wujiang District of Suzhou City (No. ZXL2021273), and The Chenzhou National Sustainable Development Agenda Innovation Demonstration Zone Provincial Special Project (No. 2023sfq11).

## Appendix A. Supporting information

Supplementary data associated with this article can be found in the online version at doi:10.1016/j.nanoen.2025.111404.

## Data availability

The data that has been used is confidential.

## References

[1] Y. Ding, Chang Zhang, L. Zhang, Y. Zhou, G. Yu, Molecular engineering of organic electroactive materials for redox flow batteries, Chem. Soc. Rev. 47 (1) (2018) 69–103.
[2] Z. Li, et al., Material design of aqueous redox flow batteries: fundamental challenges and mitigation strategies, Adv. Mater. 32 (47) (2020) 2002132.
[3] J. Winsberg, T. Hagemann, T. Janoschka, D. Martin, S. Ulrich, Redox-flow batteries: from metals to organic redox active materials, Angew. Chem. Int. Ed. 56 (3) (2017) 686–711.
[4] H. Kye, Y. Kang, D. Jang, J. Kwon, B. Kim, p-Type redox-active organic electrode materials for next-generation rechargeable batteries, Adv. Energ. Sust. Res. 3 (8) (2022) 2200030.
[5] Q. Zhao, Z. Zhu, J. Chen, Molecular engineering with organic carbonyl electrode materials for advanced stationary and redox flow rechargeable batteries, Adv. Mater. 29 (48) (2017) 1607007.
[6] X. Wei, W. Pan, W. Duan, A. Hollas, Z. Yang, B. Li, Z. Nie, J. Liu, D. Reed, W. Wang, Materials and systems for organic redox flow batteries: status and challenges, ACS Energy Lett. 2 (9) (2017) 2187–2204.
[7] H. Jiang, G. Chen, G. Hai, W. Wang, Z. Liang, L. Ding, Y. Yuan, J. Lu, H. Wang, A nitrogen battery electrode involving eight-electron per nitrogen for energy storage, Angew. Chem. Int. Ed. 62 (30) (2023) e202214601.
[8] C. Han, H. Li, R. Shi, T. Zhang, J. Tong, J. Li, B. Li, Organic quinones towards advanced electrochemical energy storage: recent advances and challenges, J. Mater. Chem. A 7 (41) (2019) 23378–23415.
[9] G. Ge, F. Li, M. Yang, Z. Zhao, G. Hou, C. Zhang, X. Li, In situ molecular reconfiguration of pyrene redox-active molecules for high-performance aqueous organic flow batteries, Adv. Mater. 36 (2025) 2412197.
[10] G. Yang, Y. Zhang, Y. Huang, M. Shakir, Y. Xu, Incorporating conjugated carbonyl compounds into carbon nanomaterials as electrode materials for electrochemical energy storage, Phys. Chem. Chem. Phys. 18 (46) (2016) 31361–31377.
[11] R. Feng, X. Zhang, V. Murugesan, A. Hollas, Y. Chen, Y. Shao, E. Walter, N. Wellala, L. Yan, M. Rosso, W. Wang, Reversible ketone hydrogenation and dehydrogenation for aqueous organic redox flow batteries, Science 372 (6544) (2021) 836–840.
[12] G. Nambafu, K. Siddharth, C. Zhang, T. Zhao, Q. Chen, K. Amine, M. Shao, An organic bifunctional redox active material for symmetric aqueous redox flow battery, Nano Energy 89 (2021) 106422.
[13] K. Lin, Q. Chen, R. Gerhardt, L. Tong, S. Kim, L. Eisenach, A. Valle, D. Hardee, R. Gordon, M. Aziz, M. Marshak, Alkaline quinone flow battery, Nature 349 (6255) (2015) 1529–1532.
[14] S. Schwan, D. Schröder, H. Wegner, J. Janek, D. Mollenhauer, Substituent pattern effects on the redox potentials of quinone-based active materials for aqueous redox flow batteries, ChemSusChem 13 (20) (2020) 5480–5488.
[15] Y. Ji, M. Goulet, D. Pollack, D. Kwabi, S. Jin, D. Porcellinis, E. Kerr, R. Gordon, M. Aziz, A phosphonate-functionalized quinone redox flow battery at near-neutral pH with record capacity retention rate, Adv. Energy Mater. 9 (12) (2019) 1900039.
[16] S. Pang, S. Jin, F. Yang, M. Alberts, L. Li, D. Xi, R. Gordon, P. Wang, M. Aziz, Y. Ji, A phenazine-based high capacity and high-stability electrochemical $CO_2$ capture cell with coupled electricity storage, Nat. Energy 8 (2023) 1126–1136.
[17] L. Wang, M. Huang, K. Wan, Z. Fu, Z. Liang, Highly soluble TEMPO-viologen bipolar molecule for ultra-stable aqueous flow batteries, Adv. Funct. Mater. 34 (11) (2024), 2310620.
[18] G. Ge, C. Mu, Y. Wang, C. Zhang, X. Li, Four-electron-transferred pyrene-4,5,9,10-tetraone derivatives enabled high-energy-density aqueous organic flow batteries, Adv. Energy Mater. 147 (13) (2025) 4790–4799.
[19] S. Pang, X. Wang, P. Wang, Y. Ji, Biomimetic amino acid functionalized phenazine flow batteries with long lifetime at near-neutral pH, Angew. Chem. Int. Ed. 60 (10) (2021) 5289–5298.
[20] M. Wu, Y. Jing, A. Wong, E. Fell, S. Jin, Z. Tang, R. Gordon, M. Aziz, Extremely stable anthraquinone negolytes synthesized from common precursors, Chem 6 (6) (2020) 1432–1442.
[21] Z. Xiang, C. Yang, W. Li, T. Xu, K. Wan, Z. Xu, Z. Liang, TEMPO microemulsion enabling extremely high capacity catholyte in aqueous organic redox flow batteries, Chem. Eng. J. 304 (2025) 121093.
[22] F. Ai, Z. Wang, N. Lai, Q. Zhou, Z. Liang, Y. Lu, Heteropoly acid negolytes for high-power-density aqueous redox flow batteries at low temperatures, Nat. Energy 7 (2022) 417–426.
[23] Z. Xiang, T. Ren, M. Huang, W. Li, L. Wang, K. Wan, Z. Liang, Manipulating aggregate electrochemistry for high-performance organic redox flow batteries, Angew. Chem. Int. Ed. 64 (4) (2025) e202416184.
[24] A. Orita, M. Verde, M. Sakai, Y. Meng, A biomimetic redox flow battery based on flavin mononucleotide, Nat. Commun. 7 (2016) 13230.
[25] X. Zhu, L. Zhang, Y. Qian, C. Zhang, G. Yu, Molecular engineering of azobenzene-based anolytes towards high-capacity aqueous redox flow batteries, Angew. Chem. Int. 59 (49) (2020) 22163–22170.
[26] C. Zhang, Z. Niu, S. Peng, Y. Peng, L. Zhang, X. Guo, Y. Zhao, G. Yu, Phenothiazine-based organic catholyte for high-capacity and long-life aqueous redox flow batteries, Adv. Mater. 31 (24) (2019) 1901052.
[27] Y. Lai, X. Li, K. Liu, W. Tang, C. Cheng, Y. Zhu, Stable low-cost organic dye anolyte for aqueous organic redox flow battery, ACS Appl. Energy Mater. 3 (3) (2020) 2290–2295.
[28] L. Lu, R. Su, Y. Ji, Y. Wang, P., A long-lived water-soluble phenazine radical tion, J. Am. Chem. Soc. 145 (2023) 5778–5785.
[29] Y. Liu, P. Zhang, Z. Wu, J. Wei, G. Ding, X. Song, J. Ma, W. Wang, Z. Jin, Screening ultra-stable (phenazine)dioxyalkanocic acids with varied water-solubilizing chain lengths for high-capacity aqueous redox flow batteries, J. Am. Chem. Soc. 146 (2024) 3293–3302.
[30] C. Wang, X. Li, B. Yu, Y. Wang, Z. Yang, H. Wang, H. Lin, J. Ma, G. Li, Z. Jin, Molecular design of fused-ring phenazine derivatives for long-cycling alkaline redox flow batteries, ACS Energy Lett. 5 (2) (2020) 411–417.
[31] S. Bailey, et al., The construction and use of potential-pH diagrams in organic oxidation-reduction reactions, J. Chem. Soc. Perkin Transit. II (5) (1983) 645–652.
[32] J. Cao, M. Tao, H. Chen, J. Xu, Z. Chen, A highly reversible anthraquinone-based anolyte for alkaline aqueous redox flow batteries, J. Power Sources 386 (2018) 40–46.
[33] J. Luo, A. Sam, B. Hu, C. Debruler, X. Wei, W. Wang, L. Liu, Unraveling pH dependent cycling stability of ferricyanide/ferrocyanide in redox flow batteries, Nano Energy 42 (2017) 215–221.
[34] C. Wang, X. Li, Y. Wang, P. Zhao, W. Yan, G. Zhu, L. Ma, B. Yu, L. Wang, G. Li, J. Liu, Z. Jin, High-performance alkaline organic redox flow batteries based on 2-hydroxy-3-carboxy-1,4-naphthoquinone, ACS Energy Lett. 3 (10) (2018) 2404–2409.
[35] M. Pan, L. Gao, J. Liang, P. Zhang, S. Lu, Y. Lu, J. Ma, Z. Jin, Reversible redox chemistry in pyrrolidinium-based TEMPO radical and extended viologen for high-voltage and long-life aqueous redox flow batteries, Adv. Energy Mater. 12 (13) (2022) 2103478.
[36] M. Pan, Y. Lu, S. Lu, B. Yu, J. Wei, Y. Liu, Z. Jin, The dual role of bridging phenylene in an extended bipyridine system for high-voltage and stable two-electron storage in redox flow batteries, ACS Appl. Mater. Interfaces 13 (37) (2021) 44174–44183.

[37] L. Tong, M.A. Goulet, D.P. Tabor, E. Kerr, D.P. Diana, R. Gordon, M. Aziz, Molecular engineering of an alkaline naphthoquinone flow battery, ACS Energy Lett. 4 (2019) 1880–1887.
[38] K. Lin, R. Gómez-Bombarelli, E. Beh, L. Tong, Q. Chen, A. Valle, R. Gordon, M. Aziz, A redox-flow battery with an alloxazine-based electrolyte, Nat. Energy 1 (2016) 16102.
[39] A. Hollas, X. Wei, V. Murugesan, Z. Nie, B. Li, D. Reed, J. Liu, V. Sprenkle, W. Wang, A biomimetic high-capacity phenazine-based anolyte for aqueous organic redox flow batteries, Nat. Energy 3 (6) (2018) 508–514.
[40] J. Xu, S. Pang, X. Wang, P. Wang, Y. Ji, Ultrastable aqueous phenazine flow batteries with high capacity operated at elevated temperatures, Joule 5 (9) (2021) 2437–2449.
[41] J. Chai, X. Wang, A. Lashgari, C. Williams, J. Jiang, A pH-neutral, aqueous redox flow battery with a 3600-cycle lifetime: micellization-enabled high stability and crossover suppression, ChemSusChem 13 (16) (2020) 4069–4077.